HHS Public Access

Author manuscript

J Mol Cell Cardiol Plus. Author manuscript; available in PMC 2023 May 18.

Published in final edited form as:

J Mol Cell Cardiol Plus. 2022 September ; 1: . doi:10.1016/j.jmccpl.2022.100012.

Evaluation of the DBA/2J mouse as a potential background strain for genetic models of cardiomyopathy

Cora C. Hart,

Young il Lee,

David W. Hammers[1],

H. Lee Sweeney[*,1]

Department of Pharmacology & Therapeutics, University of Florida College of Medicine, Gainesville, FL 32610, United States of America Myology Institute, University of Florida College of Medicine, Gainesville, FL 32610, United States of America

Abstract

The potential use of the D2.*mdx* mouse (the *mdx* mutation on the DBA/2J genetic background) as a preclinical model of the cardiac aspects of Duchenne muscular dystrophy (DMD) has been criticized based on speculation that the DBA/2J genetic background displays an inherent hypertrophic cardiomyopathy (HCM) phenotype. Accordingly, the goal of the current study was to further examine the cardiac status of this mouse strain over a 12-month period to determine if observable signs of HCM develop, including histopathology and pathological enlargement of the myocardium. Previous reports have documented heightened TGFβ signaling in the DBA2/J striated muscles, as compared to the C57 background, which, as expected, is manifested as increased cardiomyocyte size, wall thickness, and heart mass as compared to the C57 background. While normalized heart mass is larger in the DBA/2J mice, compared to age-matched C57/BL10 mice, both strains similarly increase in size from 4 to 12 months of age. We also report that DBA/2J mice contain equivalent amounts of left ventricular collagen as healthy canine and human samples. In a longitudinal echocardiography study, neither sedentary nor exercised DBA/2J mice demonstrated left ventricular wall thickening or cardiac functional deficits. In summary, we find no evidence of HCM, nor any other cardiac pathology, and thus propose that it is an appropriate background strain for genetic modeling of cardiac diseases, including the cardiomyopathy associated with DMD.

[*]Corresponding author at: 1200 Newell, Dr. ARB R5-216, Gainesville, FL 32610-0267, United States of America. lsweeney@ufl.edu (H.L. Sweeney).

[1]Equal contributions by these authors.

CRediT authorship contribution statement

Study design was contributed by CCH, YL, DWH, and HLS. Experimental procedures and data acquisition were conducted by CCH, YL, and DWH. All authors were involved in data analysis, interpretation, data presentation, and manuscript writing.

Declaration of competing interest

The authors declare that they have no known competing financial interests or personal relationships that could have appeared to influence the work reported in this paper.

Keywords

Genetic background; Cardiomyopathy; Duchenne muscular dystrophy; Echocardiography; Exercise

1. Introduction

Effective preclinical testing of potential therapeutics to treat human diseases requires the use of a model that accurately represents a disease progression and severity that is homologous to the human condition. Duchenne muscular dystrophy (DMD), for example, is the most frequently inherited pediatric neuromuscular disease. However, there are limited treatment options for this patient population despite almost three decades of preclinical and clinical research. In fact, 16 compounds have been discontinued during clinical development for DMD, and this has largely been attributed to the lack of an animal model that is representative of the human disease [1].

Indeed, the most widely used preclinical model of DMD is the *mdx* mouse on C57-based genetic backgrounds [2,3], despite their relatively mild phenotype in the limb muscles and little discernable cardiac disease until they reach old age. The increased cardiac pathology of older *mdx* mice is likely due to aging-related factors combined with dystrophin deficiency. Such age-associated factors include the diastolic dysfunction that is evident in aged wild-type mice [4]. This has led to the utilization of exogenous means, such as β-adrenergic stimulation, to worsen phenotype beyond the natural disease progression, differentiate wild-type and dystrophic cardiac function, and/or identify potential therapeutic effects [5–8]. Additional genetic manipulations, such as ablation of utrophin [9] or telomerase [10,11], have been used to worsen skeletal and cardiac muscle pathologies and decrease life expectancy of C57-based *mdx* mice. However, these manipulations do not represent genetic homologs of DMD and may mask potential therapeutic effects and/or limitations. For example, we have noted utrophin-mediated cardiac benefits following treatment with a PDE5 inhibitor [5] that would not be seen in a utrophin-deficient model. Therefore, in order to conduct translatable preclinical studies, an animal model that recapitulates both the skeletal and cardiac muscle disease progression of DMD is needed.

Recently, the D2.*mdx* mouse, consisting of the *mdx* mutation on the DBA/2J genetic background, has emerged as a severe mouse model of DMD that exhibits many features of the skeletal muscle pathology seen in human patients, including regenerative defects, progressive muscle fibrosis, muscle wasting, and reduced life-expectancy [12–17]. However, the utility of this mouse line as a suitable model to study the cardiomyopathy associated with DMD has been questioned, particularly over concerns that the DBA/2J genetic background displays inherent pathologies such as cardiac fibrosis [18,19] and a hypertrophic cardiomyopathy (HCM) [20]. In order to perform rigorous preclinical investigations, isogenic background strains devoid of any confounding pathology are necessary. Therefore, we carefully examined the cardiac status of DBA2/J (D2.WT) mice. As detailed below, we find no evidence of pre-existing cardiac pathology and thus assert that this genetic

background is a viable model to study cardiomyopathy-causing genetic diseases, such as in DMD.

2. Results

A feature of D2.WT hearts that has been interpreted as pathological, and possibly an indication of inherent HCM development, is the aberrant extra-cellular matrix (ECM) deposition [18,20]. The DBA/2J background contains a polymorphism in latent TGFβ binding protein 4 (LTBP4) that increases the susceptibility of TGFβ activation over that of mice from C57-based backgrounds [21]. While the difference between the C57 and DBA/2J LTBP4 sequence has been a point of concern, human LTBP4 more closely resembles the DBA/2J variant than C57 LTBP4 [22]. We examined whether the supposed excessive cardiac ECM deposition downstream of heightened TGFβ activity in DBA/2J background is pathological. As shown in the picrosirius red stained image of Fig. 1a–b, D2.WT hearts do exhibit a dense epicardial patch covering the right ventricle (RV), whereas other regions of the heart, particularly the left ventricle (LV) and interventricular septum (Fig. 1c–d), contain observable, but not pathological, ECM/connective tissue surrounding blood vessels and cardiomyocyte bundles. Previous investigations into the RV epicardial patch of D2.WT mice concluded that the presence of this structure does not impair cardiac function or affect mouse life span [19]. Similar epicardial regions and ventricular organization patterns as those observed in D2.WT mice can be found in heart samples from normal (cardiomyopathy-free) canines (Fig. 1e). This comparison with canines was performed because canine models of cardiomyopathies are largely considered representative of human conditions, including DMD [5,23,24] and dilated cardiomyopathy [25]. Furthermore, regions of B10.WT hearts exhibiting disorganization and perivascular ECM are also observed (Fig. 1f), demonstrating these features are not unique to the DBA/2J genetic background.

To determine how LV collagen content compares between different mouse strains and species, biochemical quantification of collagen content was performed for LV samples from C57BL/10 (B10.WT; 12 months of age; n = 6) and D2.WT mice (12 months of age; n = 6), as well as normal canines (6–12 months of age; n = 3) and humans having no history of cardiomyopathy (20–34 years of age; n = 3). Interestingly, LV collagen content (normalized to dry tissue mass) was nearly identical between B10. WT, D2.WT, and canine samples, with a slight (non-significant) increase found in human samples (Fig. 1g). This indicates that excessive and pathological levels of LV fibrosis are not a feature of D2.WT hearts.

To specifically investigate the validity of HCM development in this mouse line, we utilized in vivo echocardiography to directly assess cardiac structure and function. HCM and exercise have long been thought of as incompatible [26], therefore, a cohort of D2.WT mice with ad libitum access to a running wheel were included in this study, as previously described [27]. Running wheels were added to the cages at 5.5 weeks of age, and mice ran an average of ~5 km per day. A longitudinal study was performed in which sedentary (normal ambulation) and wheel-running mice underwent non-invasive, ultra-high frequency echocardiography bi-monthly from 4 to 12 months of age (Figs. 2 and 3).

Because a true HCM phenotype entails the progressive thickening of the left ventricle (LV) and progressive enlargement of cardiomyocytes [28], we sought to determine if either sedentary or exercised D2.WT mice exhibit such clinical features of HCM. During the first 12 months of life, we did not observe LV wall thickening or increased LV mass in D2.WT mice, even with increased physical activity (Fig. 2a–b). Wheel running induced a physiological increase in LV chamber size during diastole at 6 months of age (LV End Diastolic Volume, EDV; Fig. 2c) that normalized at the 8-month timepoint. Sedentary D2.WT mice had a slight increase in LV EDV from 6 to 10 months of age (Fig. 2c), contrary to what would be expected with a HCM phenotype. In agreement with these findings, wheel running resulted in increased cardiac reserve at 6 months of age as demonstrated by an increase in end systolic volume (ESV, Fig. 2d) and a slight decrease in ejection fraction (EF, Fig. 2e). Both ESV and EF normalized by the 8-month timepoint and remained within normal values throughout the remainder of the study. Likewise, D2.WT mice of both activity levels maintained their stroke volume (SV, Fig. 2f) throughout the study. Diastolic function was also assessed by means of color and pulsed-wave Doppler of the blood flow through the mitral valve. The myocardial performance index (MPI) is the ratio of ventricular isovolumetric and ejection time (measurements shown in Fig. 3c) and is an index of global ventricular function. An increase in this ratio is indicative of dysfunction and was not observed within the 12-month time frame of this study (Fig. 3a). Furthermore, there was no change in the LV early/late mitral valve inflow ratio (E/A, Fig. 3b). In summary, we did not observe altered cardiac function suggestive of HCM or any other underlying cardiac dysfunction in sedentary or wheel-running cohorts of D2.WT mice (Figs. 2 and 3). As shown in Fig. 4a, D2.WT mice do have a larger heart to body-size ratio, as compared to wild-type C57BL/10 (B10.WT) mice. However, the larger heart masses do not progress disproportionately with age, from 4 to 12 months of age, compared to those of B10.WT mice. Analysis of cardiomyocyte size revealed the same pattern (Fig. 4b). This is likely due to heightened TGFβ signaling, a positive regulator of cardiomyocyte size [29], in the DBA/2J genetic background [21]. The larger heart mass and cardiomyocyte size did not alter cardiac function (Table 1), which is unchanged between sedentary B10.WT and D2.WT mice at 12 months of age. These findings further indicate that spontaneous development of HCM is not a feature of D2. WT mice.

3. Discussion

The data regarding the cardiac status of the DBA/2J mouse have been contradictory [13,20]. Evidence for the manifestation of HCM in D2.WT hearts reported by Zhao et al. [20] was shown at a single time point (4 months of age) and was considered hypertrophic only in comparison with the hearts of C57BL/6 mice. While we also find that the heart mass and cardiomyocyte size of D2.WT mice are indeed larger than those of age-matched B10.WT mice (Fig. 4a–b), this does not appear to be pathological in nature, as echocardiogram-derived functional measurements are comparable between the two wild-type strains at 12 months of age (Table 1). It is suspected that the heightened TGFβ signaling exhibited by D2.WT mice during development and normal postnatal growth results in larger cardiomyocytes than those of C57 mice [21,29], but this is not a chronic driver of pathological HCM. Consistent with heightened TGFβ activity modifying organ size in

a non-pathological manner during growth and development, D2.WT skeletal muscles are smaller than their B10.WT counterparts [14], as TGFβ is a negative regulator of skeletal muscle mass [30,31]. In the context of muscular dystrophy, or any other disease setting, this heightened TGFβ activation will likely result in a more rapid and severe onset of fibrosis and disease progression. Echocardiographic findings from Coley et al. [13] show no deficits in D2.WT cardiac function from 7 to 52 weeks of age. In agreement, longitudinal data of sedentary and wheel-running D2.WT mice within the current study reveal no evidence of a progressive HCM or other underlying pathology (Figs. 1–3).

It has been asserted that D2.WT mice harbor mutations (i.e. different from the sequence expressed by C57BL/6 mice) in *Myh7* (encoding β-cardiac myosin) and myosin binding protein C (MyBP-C) that lead to HCM [20]. A close inspection of these polymorphisms reveals that this is not likely to be the case. In the case of the *Myh7* polymorphism, a new start site is established that adds five amino acids to the N-terminus without interfering with expression of the myosin. Indeed *Myh7* expression is shown in the publication by Zhao et al. [20]. Based on a large volume of work in the myosin field, tags of various size, including GFP, can be placed on the N-terminus of class II myosins (including cardiac) without any functional impact [32,33]. Furthermore, α-cardiac myosin (*Myh6*), not β-cardiac myosin, is the predominant isoform in the adult mouse heart, with the β isoform being primarily expressed during development [34].

The situation with mouse MyBP-C is even more interesting. The publication of Zhao et al. [20] asserted that the normal translation start site was lost in the DBA/2J background, which would result in a truncated protein that would be pathogenic. However, if one compares mouse and human MyBP-C sequences [35], one finds that some mouse strains, including the C57BL/6, have an N-terminal extension not found in humans: PGVTVLKMPEPGKKPVS (the mouse-specific N-terminal extension is underlined). Interestingly, the loss of the normal mouse start site will remove the mouse-specific N-terminal extension, and the protein will instead start at the normal human start site (the methionine is processed off, leaving the proline as the first amino acid in the native protein). The work of Bunch et al. [35] demonstrated that this mouse N-terminal extension, in fact, interferes with the interaction of the N-terminus of MyBP-C with myosin, therefore, its removal is likely beneficial. It appears that only certain strains of mice have gained a new start site (including SVE/129, C57BL/6, and FVB/N), while others, including the DBA/2J, have maintained (or regained) the human start site. Zhao et al. [20] also found four polymorphisms in the MyBP-C coding sequence of DBA/2J vs. C57 mice, but none of the differences have ever been linked to altered cardiac function or disease.

Herein, we demonstrate that DBA/2J mice exhibit similar perivascular connective tissue as C57 mice and healthy canines (Fig. 1a–f). Quantification of LV collagen content reveals that DBA/2J mice have no more ECM than healthy canines (Golden Retrievers; a large animal used to model DMD) and humans (Fig. 1g). Using high frequency ultrasound, we imaged the hearts of DBA/2J mice and found no LV wall thickening with wheel running (Fig. 2a). Mice of both activity levels had preserved ejection fraction (Fig. 2e) and diastolic function (Fig. 3a–b) throughout the 12 month long study. Our data and these considerations, thus,

support the use of the DBA/2J background strain for genetic mutations/manipulations that cause cardiomyopathy.

4. Methods & materials

4.1. Animals

This study used male D2.WT (DBA/2J; Jax# 000671) and B10.WT (C57BL/10ScSnJ; Jax# 000476) mice from colonies originally obtained from Jackson Laboratory. Mice were housed 1–5 mice per cage, randomly assigned into groups, provided ad libitum access to food (NIH-31 Open formulation diet; Envigo #7917), water, and enrichment, and maintained on a 12-hour light/dark system. Volitional running in D2.WT mice was implemented as previously described [27]. All animal studies were approved and conducted in accordance with the University of Florida IACUC.

4.2. Echocardiography

Transthoracic echocardiograms were performed using the Vevo 3100 pre-clinical imaging system (Fujifilm Visualsonics) with the MX-400 probe (20–46 MHz). Mice were anesthetized using 3 % isoflurane and maintained at 1.5–2 % to keep heart and respiration rates consistent among mice. Body temperature was maintained throughout imaging with the use of a heated platform and a heat lamp. Four images were acquired for each animal: B-mode parasternal long axis (LAX), B-mode short axis (SAX), M-mode SAX, and apical four-chamber view with color Doppler and pulsed-wave Doppler. M-mode SAX images were acquired at the level of the papillary muscle. Flow through the mitral valve was sampled at the point of highest velocity, as indicated by aliasing, with the pulsed-wave angle matching the direction of flow. Images were imported into Vevo LAB for analysis. Measurements of M-mode SAX and pulsed-wave Doppler images were made from three consecutive cardiac cycles between respirations.

4.3. Immunofluorescence and histological evaluations

Fresh-frozen OCT-embedded hearts were sectioned at 10 μm and fixed in ice-cold acetone. The sections were re-hydrated in PBS, blocked in 5 % BSA-PBS at room temperature and incubated with the anti-syntrophin primary antibody (1:2000; #11425; Abcam; outlines cardiomyocytes) overnight at 4 °C. Following PBS washes, sections were incubated at room temperature with a fluorescent dye-conjugated secondary antibody and coverslipped using Prolong Gold anti-fade mounting medium (ThermoFisher Scientific). Slides were visualized with a Leica DMR microscope, and images were acquired using a Leica DFC310FX camera interfaced with Leica LAS X software. Cardiomyocyte minimum ferret diameter was measured in ImageJ by investigators blinded to study groups. Picrosirius red (PSR) staining was performed as previously described [14].

4.4. Collagen assay

Snap-frozen LV samples were pulverized and disrupted with a hand homogenizer in dH_2O. A volume of 200 μL for each sample homogenate was completely desiccated by overnight incubation at 65^{O} C to obtain the dry mass of the sample to be assayed, avoiding artifacts caused by edema. Following dry mass determination, the collagen content of the samples

was measured using a colorimetric Total Collagen Assay kit (Biovision #K218) in a 96-well plate using a SpectraMax i3x multi-mode spectrophotometer (Molecular Devices). Canine samples were utilized from a previous study investigating Golden Retriever muscular dystrophy [5], and human samples were obtained from the National Disease Research Interchange (Philadelphia, PA). The subject age ranges from which these canine and human samples were procured represent windows which are expected to avoid potentially confounding variables of the myocardium, including ventricular development and age-associated factors, such as diastolic dysfunction.

4.5. Statistical analysis

Statistical analysis was performed using the appropriate form of ANOVA (one-way, two-way, or repeated measures) followed by Tukey HSD post-hoc tests ($\alpha = 0.05$). A P value <0.05 was considered significant. Data are displayed as mean ± SEM or box-and-whisker plots.

Acknowledgments

This work was funded by a Wellstone Muscular Dystrophy Cooperative Center grant (P50-AR-052646) from the NIH to HLS and DWH, a Parent Project Muscular Dystrophy grant to HLS, and a grant from the Muscular Dystrophy Association (MDA549004) to DWH. Michael Matheny, Lillian Wright, and Shailja Desai are thanked for their technical support related to this project.

Data availability

The datasets generated during and/or analyzed during the current study are available from the corresponding author on reasonable request.

References

[1]. Markati T, De Waele L, Schara-Schmidt U, Servais L. Lessons learned from discontinued clinical developments in duchenne muscular dystrophy. Front Pharmacol. 2021; 12:735912. [PubMed: 34790118]

[2]. Bulfield G, Siller WG, Wight PA, Moore KJ. X chromosome-linked muscular dystrophy (mdx) in the mouse. Proc Natl Acad Sci U S A. 1984;81(4):1189–92. [PubMed: 6583703]

[3]. Im WB, Phelps SF, Copen EH, Adams EG, Slightom JL, Chamberlain JS. Differential expression of dystrophin isoforms in strains of mdx mice with different mutations. Hum Mol Genet. 1996;5(8):1149–53. [PubMed: 8842734]

[4]. de Lucia C, Wallner M, Eaton DM, Zhao H, Houser SR, Koch WJ. Echocardiographic strain analysis for the early detection of left ventricular Systolic/Diastolic dysfunction and dyssynchrony in a mouse model of physiological aging. J Gerontol A Biol Sci Med Sci. 2019;74(4):455–61. [PubMed: 29917053]

[5]. Hammers DW, Sleeper MM, Forbes SC, Shima A, Walter GA, Sweeney HL. Tadalafil treatment delays the onset of cardiomyopathy in dystrophin-deficient hearts. J Am Heart Assoc. 2016.;5(8).

[6]. Yasuda S, Townsend D, Michele DE, Favre EG, Day SM, Metzger JM. Dystrophic heart failure blocked by membrane sealant poloxamer. Nature. 2005;436(7053):1025–9. [PubMed: 16025101]

[7]. Townsend D, Blankinship MJ, Allen JM, Gregorevic P, Chamberlain JS, Metzger JM. Systemic administration of micro-dystrophin restores cardiac geometry and prevents dobutamine-induced cardiac pump failure. Mol Ther. 2007;15(6):1086–92. [PubMed: 17440445]

[8]. Parvatiyar MS, Marshall JL, Nguyen RT, Jordan MC, Richardson VA, Roos KP, Crosbie-Watson RH. Sarcospan regulates cardiac isoproterenol response and prevents duchenne muscular dystrophy-associated cardiomyopathy. J Am Heart Assoc. 2015.;4(12).

[9]. Grady RM, Teng H, Nichol MC, Cunningham JC, Wilkinson RS, Sanes JR. Skeletal and cardiac myopathies in mice lacking utrophin and dystrophin: a model for duchenne muscular dystrophy. Cell. 1997;90(4):729–38. [PubMed: 9288752]

[10]. Sacco A, Mourkioti F, Tran R, Choi J, Llewellyn M, Kraft P, Shkreli M, Delp S, Pomerantz JH, Artandi SE, Blau HM. Short telomeres and stem cell exhaustion model Duchenne muscular dystrophy in mdx/mTR mice. Cell. 2010;143(7):1059–71. [PubMed: 21145579]

[11]. Mourkioti F, Kustan J, Kraft P, Day JW, Zhao MM, Kost-Alimova M, Protopopov A, DePinho RA, Bernstein D, Meeker AK, Blau HM. Role of telomere dysfunction in cardiac failure in Duchenne muscular dystrophy. Nat Cell Biol. 2013;15(8):895–904. [PubMed: 23831727]

[12]. Fukada S, Morikawa D, Yamamoto Y, Yoshida T, Sumie N, Yamaguchi M, Ito T, Miyagoe-Suzuki Y, Takeda S, Tsujikawa K, Yamamoto H. Genetic background affects properties of satellite cells and mdx phenotypes. Am J Pathol. 2010;176(5): 2414–24. [PubMed: 20304955]

[13]. Coley WD, Bogdanik L, Vila MC, Yu Q, Van Der Meulen JH, Rayavarapu S, Novak JS, Nearing M, Quinn JL, Saunders A, Dolan C, Andrews W, Lammert C, Austin A, Partridge TA, Cox GA, Lutz C, Nagaraju K. Effect of genetic background on the dystrophic phenotype in mdx mice. Hum Mol Genet. 2016;25(1):130–45. [PubMed: 26566673]

[14]. Hammers DW, Hart CC, Matheny MK, Wright LA, Armellini M, Barton ER, Sweeney HL. The D2.Mdx mouse as a preclinical model of the skeletal muscle pathology associated with Duchenne muscular dystrophy. Sci Rep. 2020;10(1):14070. [PubMed: 32826942]

[15]. Rodrigues M, Echigoya Y, Maruyama R, Lim KR, Fukada SI, Yokota T. Impaired regenerative capacity and lower revertant fibre expansion in dystrophin-deficient mdx muscles on DBA/2 background. Sci Rep. 2016;6:38371. [PubMed: 27924830]

[16]. Mazala DA, Novak JS, Hogarth MW, Nearing M, Adusumalli P, Tully CB, Habib NF, Gordish-Dressman H, Chen YW, Jaiswal JK, Partridge TA. TGF-beta-driven muscle degeneration and failed regeneration underlie disease onset in a DMD mouse model. JCI Insight. 2020;5(6):e135703. [PubMed: 32213706]

[17]. van Putten M, Putker K, Overzier M, Adamzek WA, Pasteuning-Vuhman S, Plomp JJ, Aartsma-Rus A. Natural disease history of the D2. FASEB J. 2019;33(7):8110–24. [PubMed: 30933664]

[18]. Hakim CH, Wasala NB, Pan X, Kodippili K, Yue Y, Zhang K, Yao G, Haffner B, Duan SX, Ramos J, Schneider JS, Yang NN, Chamberlain JS, Duan D. A five-repeat micro-dystrophin gene ameliorated dystrophic phenotype in the severe DBA/2J-mdx model of duchenne muscular dystrophy. Mol Ther Methods Clin Dev. 2017;6: 216–30. [PubMed: 28932757]

[19]. Nabors CE, Ball CR. Spontaneous calcification in hearts of DBA mice. Anat Rec. 1969; 164(2):153–61. [PubMed: 4181974]

[20]. Zhao W, Zhao T, Chen Y, Zhao F, Gu Q, Williams RW, Bhattacharya SK, Lu L, Sun Y. A murine hypertrophic cardiomyopathy model: the DBA/2J strain. PLoS One. 2015;10(8): e0133132. [PubMed: 26241864]

[21]. Heydemann A, Ceco E, Lim JE, Hadhazy M, Ryder P, Moran JL, Beier DR, Palmer AA, McNally EM. Latent TGF-beta-binding protein 4 modifies muscular dystrophy in mice. J Clin Invest. 2009;119(12):3703–12. [PubMed: 19884661]

[22]. Ceco E, Bogdanovich S, Gardner B, Miller T, DeJesus A, Earley JU, Hadhazy M, Smith LR, Barton ER, Molkentin JD, McNally EM. Targeting latent TGFbeta release in muscular dystrophy. Sci Transl Med. 2014;6(259):259ra144.

[23]. Guo LJ, Soslow JH, Bettis AK, Nghiem PP, Cummings KJ, Lenox MW, Miller MW, Kornegay JN, Spurney CF. Natural history of cardiomyopathy in adult dogs with Golden retriever muscular dystrophy. J Am Heart Assoc. 2019;8(16):e012443. [PubMed: 31411085]

[24]. Kornegay JN, Bogan JR, Bogan DJ, Childers MK, Li J, Nghiem P, Detwiler DA, Larsen CA, Grange RW, Bhavaraju-Sanka RK, Tou S, Keene BP, Howard JF Jr, Wang J, Fan Z, Schatzberg SJ, Styner MA, Flanigan KM, Xiao X, Hoffman EP. Canine models of duchenne muscular dystrophy and their use in therapeutic strategies. Mamm Genome. 2012;23(1–2):85–108. [PubMed: 22218699]

[25]. Recchia FA, Lionetti V. Animal models of dilated cardiomyopathy for translational research. Vet Res Commun. 2007;31(Suppl 1):35–41. [PubMed: 17682844]

[26]. Maron BJ, Ackerman MJ, Nishimura RA, Pyeritz RE, Towbin JA, Udelson JE. Task force 4: HCM and other cardiomyopathies, mitral valve prolapse, myocarditis, and Marfan syndrome. J Am Coll Cardiol. 2005;45(8):1340–5. [PubMed: 15837284]

[27]. Hammers DW, Sleeper MM, Forbes SC, Coker CC, Jirousek MR, Zimmer M, Walter GA, Sweeney HL. Disease-modifying effects of orally bioavailable NF-kappaB inhibitors in dystrophin-deficient muscle. JCI Insight. 2016;1(21):e90341. [PubMed: 28018975]

[28]. Marian AJ. Molecular genetic basis of hypertrophic cardiomyopathy. Circ Res. 2021;128 (10):1533–53. [PubMed: 33983830]

[29]. Rosenkranz S TGF-beta1 and angiotensin networking in cardiac remodeling. Cardiovasc Res. 2004;63(3):423–32. [PubMed: 15276467]

[30]. Hammers DW, Merscham-Banda M, Hsiao JY, Engst S, Hartman JJ, Sweeney HL. Supraphysiological levels of GDF11 induce striated muscle atrophy. EMBO Mol Med. 2017;9(4):531–44. [PubMed: 28270449]

[31]. Mendias CL, Gumucio JP, Davis ME, Bromley CW, Davis CS, Brooks SV. Transforming growth factor-beta induces skeletal muscle atrophy and fibrosis through the induction of atrogin-1 and scleraxis. Muscle Nerve. 2012;45(1):55–9. [PubMed: 22190307]

[32]. Wolny M, Colegrave M, Colman L, White E, Knight PJ, Peckham M. Cardiomyopathy mutations in the tail of beta-cardiac myosin modify the coiled-coil structure and affect integration into thick filaments in muscle sarcomeres in adult cardiomyocytes. J Biol Chem. 2013;288(44):31952–62. [PubMed: 24047955]

[33]. Kengyel A, Wolf WA, Chisholm RL, Sellers JR. Nonmuscle myosin IIA with a GFP fused to the N-terminus of the regulatory light chain is regulated normally. J Muscle Res Cell Motil. 2010;31(3):163–70. [PubMed: 20711642]

[34]. Ng WA, Grupp IL, Subramaniam A, Robbins J. Cardiac myosin heavy chain mRNA expression and myocardial function in the mouse heart. Circ Res. 1991;68(6):1742–50. [PubMed: 2036722]

[35]. Bunch TA, Lepak VC, Kanassatega RS, Colson BA. N-terminal extension in cardiac myosin-binding protein C regulates myofilament binding. J Mol Cell Cardiol. 2018; 125:140–8. [PubMed: 30359561]

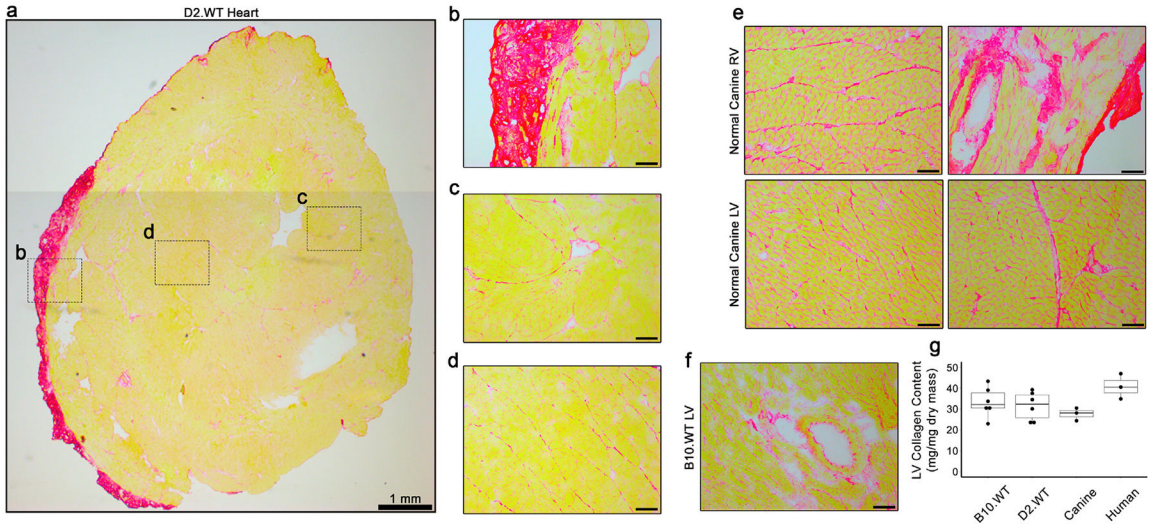

Fig. 1.

Comparative analysis of left ventricular collagen content. (a) Representative picrosirius red staining of a 12 mo D2.WT heart cross-section reveals (b) robust collagen staining at the epicardium of the right ventricle (RV) and non-pathological connective tissue organization within the (c) left ventricle (LV) free-wall and (d) interventricular septum, particularly in areas containing major blood vessels. (e) Images of RV and LV samples from 12 mo normal canine hearts reveal similar features as the D2.WT hearts, including regions of dense collagen content of the RV free-wall and perivascular connective tissue. (f) The vessel-associated collagen detection by picrosirius red staining is also featured in the hearts of 12 mo B10.WT mice. (g) Biochemical analysis of LV collagen content from 12 mo B10.WT (n = 6), 12 mo D2.WT (n = 6), 6–12 mo normal canine (n = 3), and 20–34 yo human hearts (n = 3). Data were analyzed using ANOVA. No significant differences between groups were found. Scale bars indicate 100 μm, unless otherwise noted.

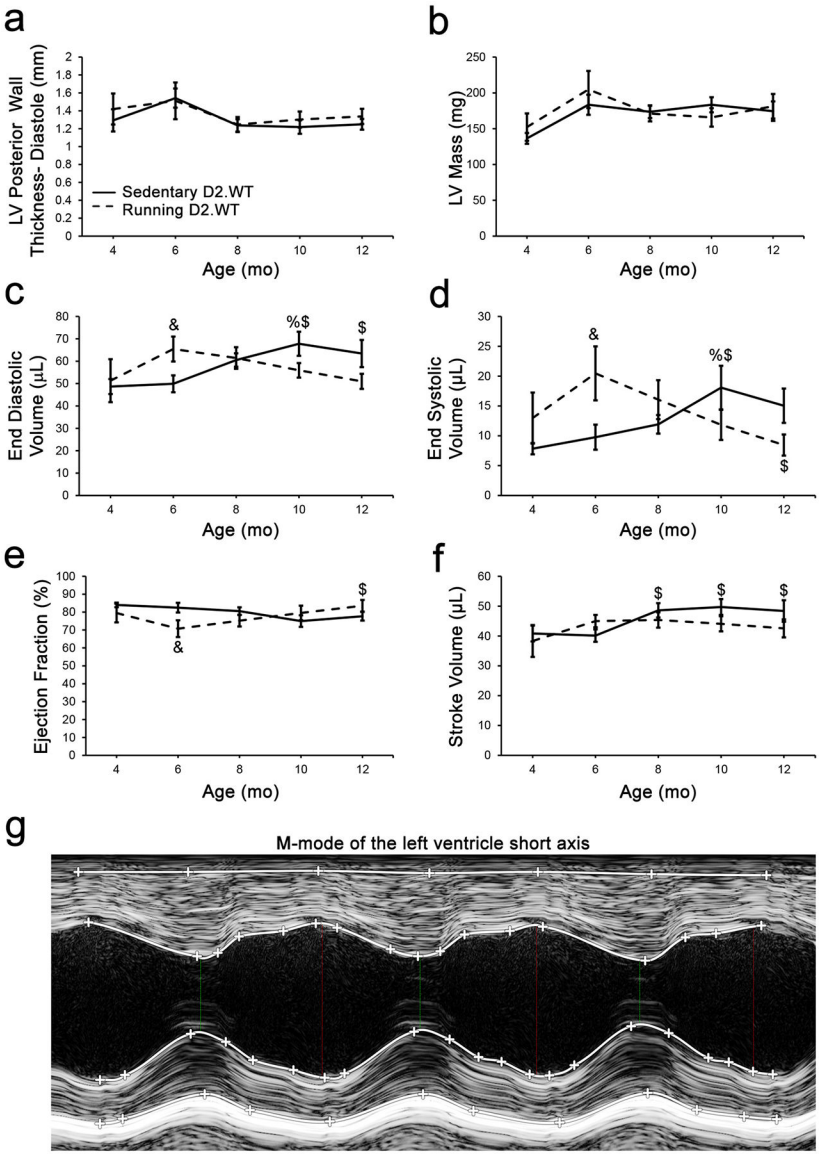

Fig. 2.

The DBA/2J genetic background does not exhibit hypertrophic cardiomyopathy. Male DBA/2J (D2.WT) mice of sedentary (n = 10) and volitional wheel-running (n = 7) cohorts were followed longitudinally between the ages of 4- and 12-months using echocardiography to determine if this mouse strain exhibits a progressive cardiomyopathy resembling hypertrophic cardiomyopathy. Cardiac functional parameters of (a) diastolic left ventricle (LV) posterior wall thickness, (b) LV mass, (c) end diastolic volume, (d) end systolic volume, (e) ejection fraction, and (f) stroke volume, from these mouse cohorts are displayed and do not suggest a hypertrophic cardiomyopathy develops in this mouse strain during the ages investigated in this study. These measurements were acquired from m-mode images of the LV short axis at the level of the papillary muscle (g). Data were analyzed using two-factor repeated measures ANOVA (Tukey post-hoc tests; $\alpha = 0.05$); $^{\%}P < 0.05$ vs.

group-matched 4 mo values; $^{\$}P < 0.05$ vs. group-matched 6 mo values; $^{\&}P < 0.05$ vs. age-matched sedentary values.

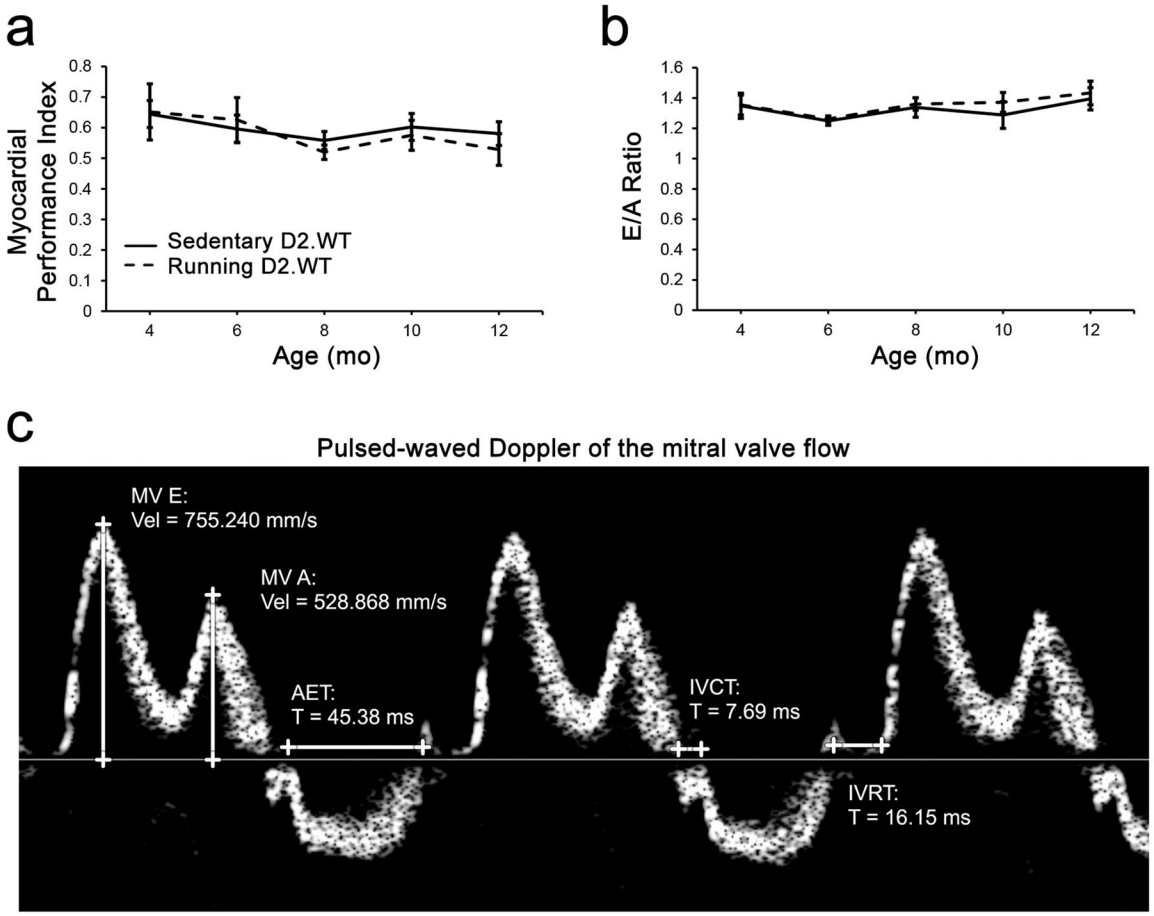

Fig. 3.

Diastolic function is maintained in wheel-running D2.WT mice. Diastolic function was assessed by visualizing the blood flow through the mitral valve in a 4-chamber apical view image using color Doppler. Myocardial performance index (a) and mitral valve E/A ratio (b) were unchanged from 4 to 12 months of age and were not different between cohorts. These measurements were obtained from pulsed-wave Doppler images (c) obtained at the maximum velocity of blood flow through the mitral Valve. Data were analyzed using two-factor repeated measures ANOVA (Tukey post-hoc tests; $\alpha = 0.05$); however, significance was not observed.

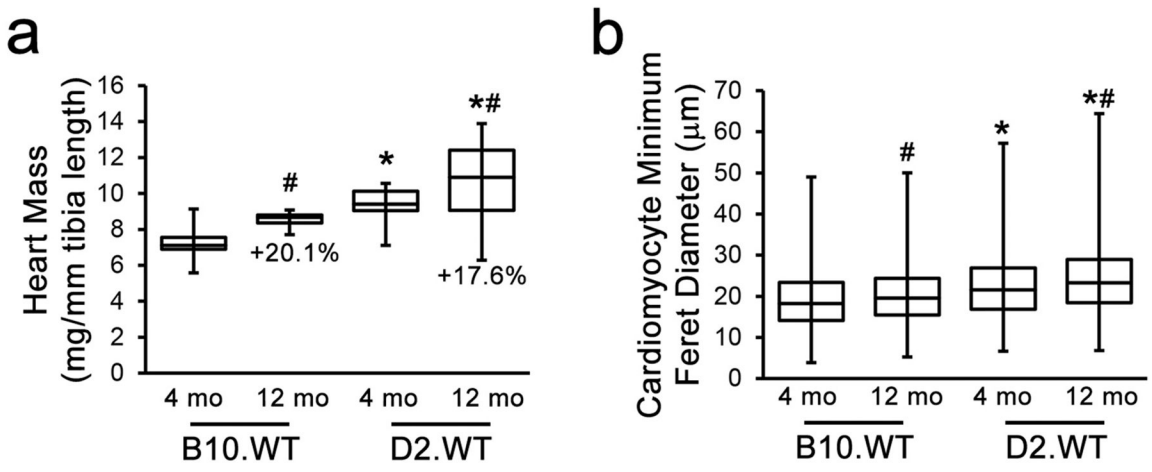

Fig. 4.

Heart size in B10.WT and D2.WT mice. A comparison of (a) heart mass (normalized to tibia length; n = 17, 10, 17, and 18 respectively) and (b) cardiomyocyte size (n = 1971, 1996, 1655, and 1527 cardiomyocytes respectively) was performed between 4- and 12-month-old C57BL/10 (B10.WT) and D2.WT mice to identify how heart size progresses between the two genetic backgrounds. Data were analyzed using two-factor ANOVA (Tukey post-hoc tests; $\alpha = 0.05$); *$P < 0.05$ vs. age-matched B10.WT values; $^{\#}P < 0.05$ vs. strain-matched 4 mo values.

Table 1

Echocardiogram measurements in B10.WT and D2.WT mice.

	B10.WT	D2.WT
Heart rate (bpm)	463.24 ± 11.94	429.13 ± 15.22
LVAW;s (mm)	1.78 ± 0.09	2.03 ± 0.10
LVAW;d (mm)	1.17 ± 0.05	1.33 ± 0.08
LVPW;s (mm)	1.72 ± 0.09	1.81 ± 0.06
LVPW;d (mm)	1.18 ± 0.09	1.25 ± 0.06
EDD (mm)	3.65 ± 0.06	3.80 ± 0.15
ESD (mm)	2.08 ± 0.07	2.07 ± 0.16
EDV (μL)	56.29 ± 2.19	63.43 ± 6.07
ESV (μL)	14.23 ± 1.23	15.04 ± 2.87
SV (μL)	42.06 ± 2.13	48.39 ± 3.59
CO (mL/min)	19.44 ± 0.94	20.47 ± 1.20
EF (%)	74.64 ± 2.16	77.69 ± 2.43
FS (%)	42.93 ± 1.98	46.24 ± 2.26
MV E (mm/s)	699.35 ± 18.17	729.24 ± 19.10
MV A (mm/s)	597.93 ± 36.53	534.13 ± 22.66
MV E/A	1.19 ± 0.07	1.39 ± 0.07
AET (ms)	47.75 ± 1.13	46.48 ± 1.32
IVCT (ms)	12.31 ± 1.08	10.34 ± 1.18
IVRT (ms)	15.79 ± 0.50	16.41 ± 1.02
LV MPI IV	0.59 ± 0.02	0.58 ± 0.04

Cardiac function was assessed in 12-month-old D2.WT (n = 10) and B10.WT (n = 6) mice using LV short axis m-mode images and pulsed-wave Doppler of the flow through the mitral valve. Heart Rate (beats per second, BPM), LVAW; s (LV anterior wall thickness during systole, mm), LVAW;d (LV anterior wall thickness during diastole, mm), LVPW;s (LV posterior wall thickness during systole, mm), LVPW;d (LV posterior wall thickness during diastole, mm), EDD (end diastolic diameter, mm), ESD (end systolic diameter, mm), EDV (end diastolic volume, μL), ESV (end systolic volume, μL), SV (stroke volume, μL), CO (cardiac output, mL/min), EF (ejection fraction, %), FS (fractional shortening, %), MV E (mitral valve early flow velocity, mm/s), MV A (MV atrial flow velocity, mm/s), MV E/A (MV early/late flow ratio), AET (aortic ejection time, ms), IVRT (isovolumic relaxation time, ms), IVCT (isovolumic contraction time, ms), LV MPI IV (LV myocardial performance index, isovolumic). Data were analyzed using student's *t*-test and no significance was found.